AIAA JOURNAL
Vol. 34, No. 10, October 1996

Large-Scale Structure Evolution in Supersonic Interacting Shear Layers

N. T. Clemens,* S. P. Petullo,† and D. S. Dolling‡
University of Texas at Austin, Austin, Texas 78712-1085

An experimental investigation is made of the evolution of the large-scale structures in a flow consisting of two planar turbulent shear layers formed by a Mach-3 planar jet bounded by a Mach-5 freestream. The flow is characterized by two planar shear layers at a convective Mach number of 0.28 that are independent in the near field but that interact farther downstream. Measurements were made using fast-response hot-wire probes and planar laser scattering from a condensed alcohol fog. The hot-wire data were used to calculate power spectra and cross correlations from which large-scale-structure length scales and orientation were inferred. The images reveal roller-like structures, but they do not appear as dominant or as coherent compared with low-Mach-number shear layers at a similar Reynolds number. The hot-wire data confirm the relatively unorganized and three-dimensional nature of the independent shear layers. In the far field, the visualizations reveal that the shear layers interact to form a more organized structure, similar to vortex shedding in incompressible turbulent wakes. These organized structures result in a distinct peak in the power spectrum and larger spanwise coherence lengths than for the independent shear layer.

Nomenclature

a_1, a_2 = high- and low-speed freestream speed of sound, respectively
f = frequency
$G(f)$ = power spectral density, V^2/Hz
H = boundary-layer shape factor
M_c = convective Mach number
M_1, M_2 = high- and low-speed freestream Mach number, respectively
M_∞ = freestream Mach number
N = number of events per bin
N_T = total number of events
P_t = pitot pressure
Re_θ = Reynolds number based on momentum thickness
R_{12} = normalized cross-correlation coefficient
S = large-scale-structure streamwise spacing
U_c = convection velocity
U_1, U_2 = high- and low-speed freestream velocity, respectively
W = histogram bin width
x = streamwise distance from model trailing edge
y = vertical location from top surface of model
y_o = vertical coordinate of the shear-layer centerline
z = spanwise coordinate
β = large-scale-structure angle in the x-y plane
ΔU = velocity difference, $U_2 - U_1$
Δy = hot-wire probe vertical wire spacing
Δz = hot-wire probe spanwise wire spacing
δ = boundary-layer velocity thickness (99%)
δ_{pt} = shear-layer pitot thickness (5–95%)
δ_{vis} = shear-layer visual thickness
δ^* = boundary-layer displacement thickness
θ = boundary-layer momentum thickness
θ_o = momentum thickness at the shear-layer origin
ν = kinematic viscosity
Π = boundary-layer wake parameter
σ = rms of anemometer output fluctuations
σ^2 = signal variance
σ_τ = standard deviation of time delay
τ = cross-correlation time delay
τ_p = time delay at the peak cross correlation
τ_2 = time delay at the secondary correlation peak
$\bar{\tau}$ = mean time delay
χ = large-scale-structure angle in the x-z plane

Presented as Paper 93-0545 at the AIAA 31st Aerospace Sciences Meeting, Reno, NV, Jan. 11–14, 1993; received Feb. 10, 1994; revision received Feb. 21, 1996; accepted for publication March 2, 1996.

*Assistant Professor, Department of Aerospace Engineering and Engineering Mechanics. Member AIAA.
†Graduate Research Assistant, Department of Aerospace Engineering and Engineering Mechanics; currently Research Engineer, Southwest Research Institute, San Antonio, TX 78228-0510. Member AIAA.
‡Professor, Department of Aerospace Engineering and Engineering Mechanics. Associate Fellow AIAA.

Introduction

OVER the past decade, interest in the development of supersonic combustion engines has driven extensive research into the structure of supersonic turbulent shear flows. Most recent studies have concentrated on planar shear layers because of their relative simplicity, although actual supersonic combustion engines will have significantly more complex flowfields.[1,2] In the present work, the organization of the large-scale structure is investigated in a flow composed of two supersonic shear layers that are independent in the near field, but then interact downstream.

Studies of compressible shear layers have defined M_c as the most relevant parameter with which to quantify compressibility.[3,4] [For freestreams with equal ratio of specific heats, $M_c = \Delta U/(a_1 + a_2)$.] Increasing M_c is associated with reduced shear-layer growth rates,[3–8] reduced turbulent fluctuations,[5,6,9] and large-scale structure that is more three-dimensional and disorganized than under incompressible conditions.[7,10–12]

As part of a study of supersonic base flows, the interaction between two planar compressible shear layers also has been investigated.[13,14] In the case of base flows, however, the interaction between the shear layers is complicated by the fact that the interaction region is a region of recompression and is highly unsteady. Flow visualization of the interaction region reveals structures that are apparently more organized than the upstream shear layers, but they do not appear to be part of an identifiable vortex street.[14] The absence of a vortex street is typical of supersonic wakes originating from both bluff[15] and thin[16,17] trailing edges when splitter plate boundary layers are fully turbulent. Interacting low-speed shear layers were studied by Weir et al.,[18] who found that the transport of Reynolds stress was considerably modified in the interaction region.

The flow configuration for the present study consists of two supersonic shear layers formed by two high-Mach-number streams ($M_1 = 5$, $M_2 = 3$), but at the low convective Mach number of 0.28.

This shear-layer configuration is simpler than the base-flow case because the interaction region does not suffer from recompression effects. Over the past several years, experimental investigations have been made of the development and structure of this same flowfield. Shau[19] and Shau et al.[20] characterized the growth rate and mean two-dimensionality of the shear layers. Shau also computed average large-scale-structure inclination angles from two-point cross correlations, which showed increasing structure angles and increasing organization with increasing streamwise location.

The present measurements are improved by using only less intrusive, higher-frequency-response hot wires, and flow visualization using planar laser scattering (PLS) from a condensed alcohol fog. The PLS imaging was used to visualize shear-layer structures and to determine structure velocities and inclination angles. The signals from the hot wires were used to examine the degree of organization as determined from cross correlations and histograms of structure inclination angle. For comparison with the degree of organization found in the shear layer, the structure of the undisturbed (empty wind tunnel) Mach-5 turbulent boundary layer on the tunnel floor also was investigated. The present study provides new data that show that the increasing organization reported by Shau et al.[20] results from the interaction between the two shear layers.

Experimental Program

The experiments were conducted in the Mach 5 blowdown wind tunnel of the University of Texas Wind Tunnel Laboratories. The test section is 15.24 cm wide × 17.75 cm high and is 68.6 cm long. Nominal stagnation conditions for the Mach-5 stream were 2.096×10^6 N/m^2 ± 1% and 350 K ± 2%. The model is shown in Fig. 1. Details of its design and the shear layer and tunnel air supplies are described by Shau.[19] Previous studies have examined the entire shear-layer flowfield and initial conditions in detail, and the mean flow properties are well documented.[19,20] At the shear-layer origin, the Mach-5 boundary layer is fully turbulent and characterized by the following properties: $M_\infty = 4.90$, $\delta = 4.7$ mm, $\delta^* = 2.5$ mm, $\theta = 0.21$ mm, $H = 11.6$, $Re_\theta = 9.6 \times 10^3$, and $\Pi = 0.84$. Because of its small thickness ($\delta < 0.6$ mm) the Mach-3 boundary-layer profile was not surveyed; however, it is believed to be laminar, based on the Reynolds number.

The shear-layer structure was investigated with the hot wires at $x = 17.8$ and 48.3 cm as shown in Fig. 1, and using PLS imaging over the range $x = 33$–38 and 43–50.5 cm. Mean pitot surveys were conducted for verification of the flowfield conditions and as an aid in locating subsequent hot-wire probe positions. At both locations, the dual hot-wire probes were centered at five vertical (y) positions. The mean pitot profiles, hot-wire measurement locations (a–e), and coordinate system origin are illustrated in Fig. 1. In the case of the dual vertical wire probes, each location corresponds to the midpoint of the vertical wire spacing. Also indicated in Fig. 1 for each pitot survey is δ_{pt} and y_o.

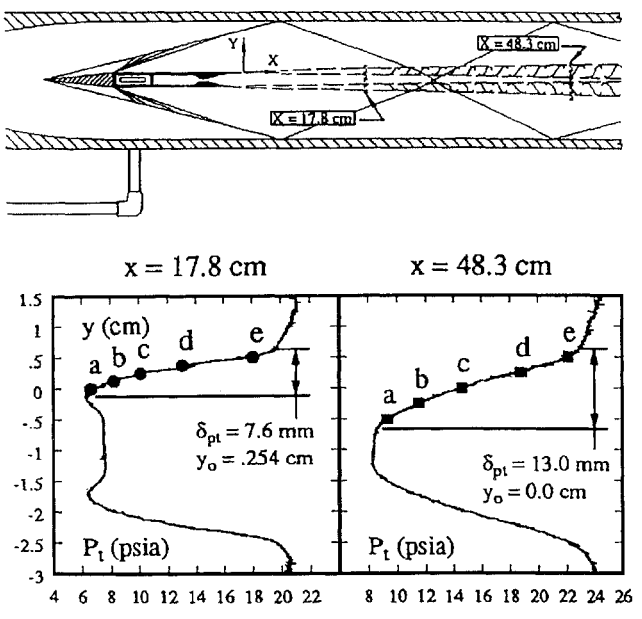

Fig. 1 Pitot surveys and measurement locations.

As in earlier work,[20] mean shear-layer pitot pressure profiles along the tunnel centerline were obtained using a pitot probe of conventional design incorporating a remotely mounted Kulite pressure transducer (Model XCQ-062-50A). Output from the transducer was low-pass filtered with the cutoff frequency set at 20 Hz and digitized using a LeCroy Model 6810 Waveform Recorder employing a 12-bit A/D converter. The mean pitot pressure evolution and shear-layer thickness variation streamwise are elsewhere.[20] In the present study, the same method was used, but measurements were made only at $x = 17.8$ cm (848 θ_o) and $x = 48.3$ cm (2300 θ_o).

Three configurations of multiwire hot-wire probes, fabricated in-house, were used. The shear-layer structure at the two streamwise stations and the undisturbed Mach-5 boundary-layer structure (for comparison) were investigated at five vertical locations using a dual-wire probe. Wire spacings of 2.6 and 4.5 mm were employed at $x = 17.8$ cm, which corresponds to $\Delta y/\delta_{pt}$ ratios of 0.35 and 0.60, respectively. At $x = 48.3$ cm, wire spacings of 4.5 and 8 mm were used so that the same two shear-layer thickness ratios ($\Delta y/\delta_{pt} = 0.35$ and 0.60) were obtained. When using dual-wire probes resulting in a $\Delta y/\delta_{pt}$ of 0.60, data were acquired only at vertical location c. The spanwise shear-layer structure at $x = 17.8$ and 48.3 cm was investigated with a six wire rake. Because of data acquisition constraints, only two wires were active in any given run when using this rake.

Each hot-wire probe was connected to two constant-temperature anemometers (DANTEC) with standard bridges (DISA-55M10 with bridge ratio 20:1) and operated at an overheat ratio of 0.68 to maintain the tungsten filament at a temperature just below 600 K. The 5-μm-diam wire filaments (with a length/diameter ratio of 200) were each tuned to 120-kHz frequency response. The hot-wire signals were low-pass filtered at 100 kHz and sampled at 5 MHz per channel. Because of the high mean velocity of the shear layers, the 100-kHz bandwidth is sufficient to resolve only the large-scale fluctuations, which are of primary interest in this study. The exceptionally high digitization rate (5 MHz) affords a 0.2-μs time resolution and results in well-resolved timing and structure-angle histograms. On each channel, 2048 records of data (1024 data points per record) were collected. No calibration of the hot wires was performed because the interest was on the time delay between events on the two channels rather than absolute mass-flux fluctuations. If a strong concentration of energy exists at a given frequency, the spectrum of the voltage fluctuations will indicate this just as clearly as the spectrum of the mass-flux fluctuations.[21]

The PLS technique is similar to the vapor screen technique developed by McGregor[22] and has recently been applied in several supersonic shear-layer studies.[7,10,11] It involves injecting ethanol liquid upstream of the plenum using three fine-spray atomizing nozzles. The ethanol droplets evaporate before reaching the nozzle and then recondense because of the rapid cooling associated with the expansion through the supersonic nozzle. The result is an extremely fine fog that has been measured in another facility to be less than 0.2 μm,[23] which is more than sufficient for the droplets to track the large-scale turbulent fluctuations.[24] Although both freestreams are seeded with vapor and both originate from supersonic nozzles, the scattered light on the high-speed side was much larger, thus providing sufficient contrast for flow visualization.

The PLS technique uses a frequency-doubled Nd:YAG laser (Lumonics YM600) operating at 10 Hz, 60 mJ per pulse, and with a flow-stopping pulse duration of 10 ns. In some cases the laser was double pulsed with temporal separation between pulses of 15 μs. The laser beam was formed into a sheet approximately 15-cm wide and 500 μm thick. The scattered light was collected using a charge-coupled device video camera (Cohu 4990) coupled to a f1.2, 50-mm camera lens. For the double-pulse imaging, a frame straddling technique was used in which each pulse was placed in a different video field. Because of optical access limitations, the probe and image data could not be obtained at the same upstream location. A total ensemble of 180 images was obtained for each case, which were digitized to 512 × 240 resolution using a frame grabber

(DataTranslation DT 2851) that was installed in a 486-66 MHz personal computer.

Analysis Techniques

Statistical and Time-Series Analysis of the Hot-Wire Data

The mean, standard deviation, skewness and flatness coefficients, as well as amplitude probability density distributions of the hot-wire signals were calculated to examine the general character of the data and for comparison with earlier work. Power spectra were calculated using the fast Fourier transform (FFT) technique, and cross correlations of the two-point hot-wire measurements were calculated from the inverse FFT of the cross-spectral density function[25] to provide a measure of the average structure inclination angle in the x-y plane, β, and of the average spanwise structure oblique angle in the x-z plane, χ. From the time delay τ_p at the peak cross-correlation coefficient, the structure angle can be estimated from $\beta = \tan^{-1}[\Delta y/(U_c\tau_p)]$ (in the x-y plane) and $\chi = \tan^{-1}[(U_c\tau_p)/\Delta z]$ (in the x-z plane). Because the velocities of the high- and low-speed streams are 760 and 660 m/s, respectively, an average value (710 m/s) was assumed for the large-scale-structure convection velocity. The assumed value is not critical because an uncertainty in convection velocity of ±30 m/s results in an uncertainty in structure angle of only ±1 deg at a sampling rate of 5 MHz.

Conditional Cross-Correlation Analysis

As stated previously, the main objective of the present study is to provide a measure of the degree of organization of the shear-layer structure. To obtain a distribution of angles in addition to the average deduced from standard cross correlations, a conditional cross-correlation algorithm was developed and presented in detail.[26] The conditional cross-correlation method takes advantage of the extremely well-resolved hot-wire fluctuations obtained with a 5-MHz sampling rate. As the pair of hot wires is translated from the lower part of the shear layer (near location a in Fig. 1) to the upper part (location e), the skewness of the signal changes from positive to negative, and, particularly at the edges of the shear layer, large amplitude fluctuations are more prominent and are easily distinguished from low-level freestream fluctuations.

The basic steps in the analytical procedure are event detection, cross correlation, and histogram construction. Events are detected on the basis of the trigger channel signal skewness and threshold level. A minimum event length of 5 μs was set so as to include events only with frequency up to the low-pass filter setting of 100 kHz. When an event is detected, data strings of length three times the event time duration are extracted from channels 1 and 2. These two data strings are cross correlated algebraically, and the time delay corresponding to the peak correlation coefficient is found. In nearly all cases, a well-defined peak occurs. This process is continued for all events detected, and a histogram of time delays is constructed that can be subsequently converted to structure angles. However, because of the use of the inverse tangent function in determining the structure angle, equal increments in time do not result in equal increments in angle, and the histograms computed from the conditional cross-correlation algorithm are best presented as time-delay histograms. Also computed by the algorithm is an uncorrelated level obtained from analysis of the hot-wire data with channel 2 shifted one record relative to channel 1. As expected, the uncorrelated level is basically flat and is indicated as a horizontal line in the histograms.

The sensitivity of the conditional cross-correlation algorithm to threshold level and number of records analyzed was examined previously.[26] Results showed that changes in threshold setting about the nominal value or use of a different number of records (above a minimum) had little effect on histogram shape or levels.

Results

PLS Imaging

Two uncorrelated PLS images taken at the $x = 36$ cm station are shown in Fig. 2. In this region the shear layers are still independent, the local Reynolds number $Re_\delta = \Delta U \delta_{vis}/\nu = 4 \times 10^4$ and $x = 1600\,\theta_o$. From the entire ensemble of 180 images, it can be concluded that roller-like structures are present (Fig. 2, top), but they are not a dominant feature because they appear in only about 15% of the images. The remainder of the images appear to be quite indistinct and unorganized. This trend is different from the highly organized structure found by Clemens and Mungal[7] at the same M_c, but at an order-of-magnitude larger Reynolds number. The double-pulse images (not shown) indicate that the structures exhibit little distortion (i.e., primarily translation) as they convect approximately one shear-layer thickness downstream. Also apparent in about 40–50% of the images is that a characteristic angle often can be observed, as seen in Fig. 2 (top). The characteristic angles, which are typically associated with the upstream edges of the large-scale structures, were measured for the ensemble of images. A histogram of the results reveals an approximately Gaussian distribution, with a mean angle of about 28 deg and a standard deviation of about 6 deg.

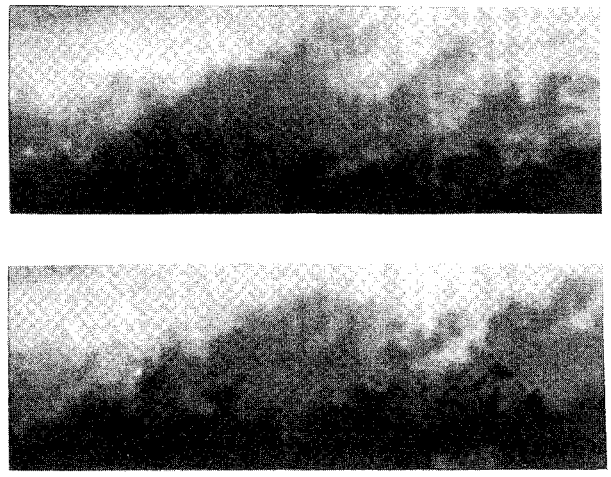

Fig. 2 Two uncorrelated PLS images. The field of view spans the range x = 34–38.5 cm, the flow is from left to right, and the high-speed stream is shaded light.

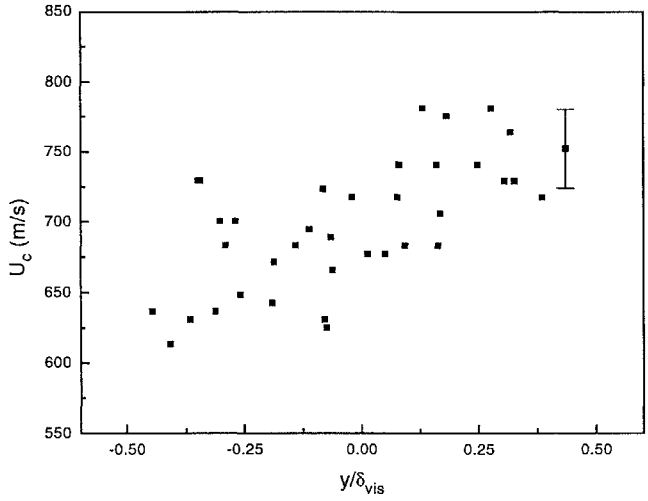

Fig. 3 Structure convection velocities determined from the PLS images (x = 36 cm).

The double-pulse image pairs were used to determine structure convection velocities by tracking the displacement of a feature that could be identified in both images. The distance traveled and the known time between the laser pulses (15 μs) was then used to calculate the convection velocity. Velocity measurements were made at several cross-stream locations across the shear layer, as shown in Fig. 3. The error bar in Fig. 3 applies to all data points and reflects the uncertainty in the laser pulse separation and in identifying the distance between structures in each of the double-pulse image sets. The figure shows that different parts of a structure convect at different velocities. This has been shown previously in incompressible[27] and compressible shear layers,[12,28,29] where structure convection velocities varied across the shear layer.

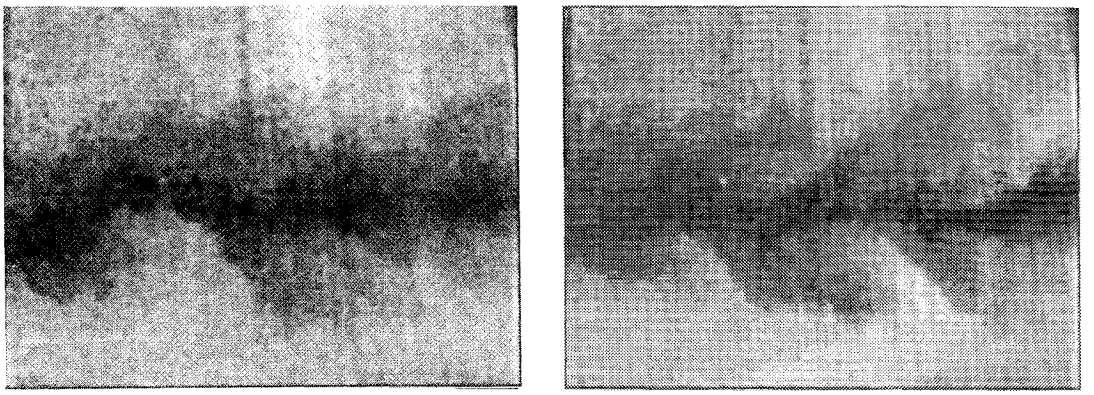

Fig. 4 Two uncorrelated PLS images. The field of view spans the range x = 43–50.5 cm, the flow is from left to right, and the high-speed streams at top and bottom are shaded light.

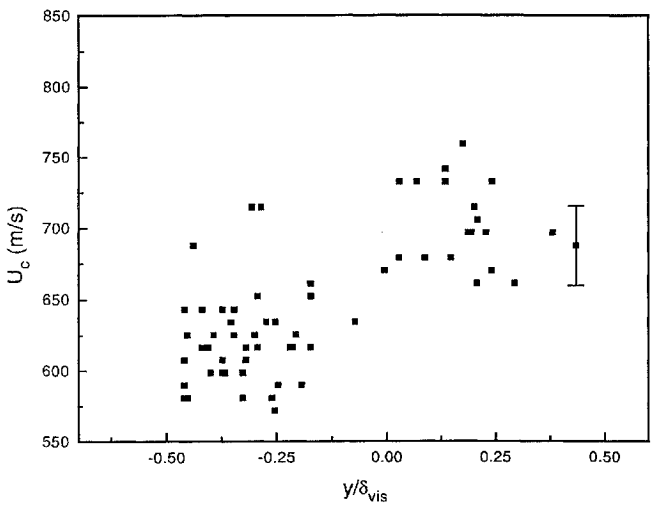

Fig. 5 Structure convection velocities determined from the PLS images (x = 48 cm).

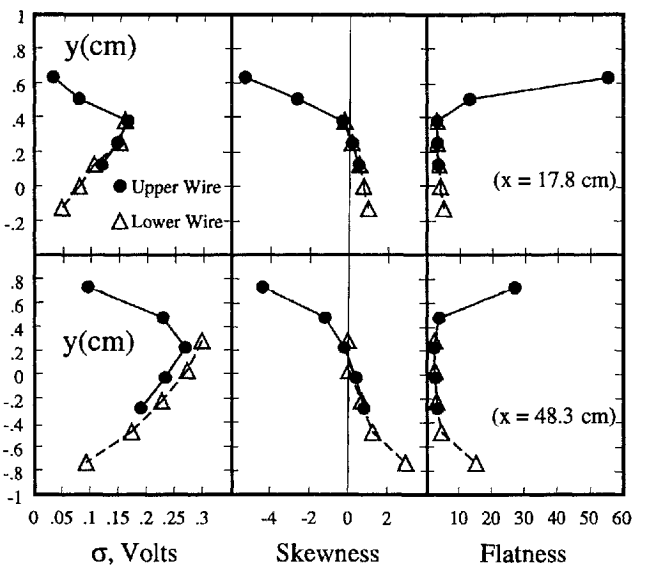

Fig. 6 Voltage fluctuation statistics across the shear layer.

In Fig. 4, two uncorrelated images were taken at the $x = 48$ cm station where $Re_\delta = 6 \times 10^4$ and $x = 2300\,\theta_o$. These images are characteristic of the majority of the images where a sinuous pattern is evident, indicating the development of a wake-like instability that appears to be characterized by antisymmetric vortex shedding. The structures that develop are highly organized and correlated across both shear layers. The double-pulse images (not shown) reveal that the structures primarily translate, exhibiting little distortion. Characteristic angles are observed often and, as at the upstream station, they were measured for the image ensemble. These angles also were associated with the upstream edges of the structures, as seen in Fig. 4 (right). In this case the mean angle was 42 deg (with a standard deviation of 7 deg), which is substantially larger than for the upstream independent shear layer. The convective velocity distribution across the flow also was measured for the image ensemble and is shown in Fig. 5, where the velocities also are seen to vary across the shear layer and are approximately bounded by the high- and low-speed freestream velocities.

Hot-Wire Statistics

Figure 6 presents rms, skewness, and flatness distributions in the y direction across the upper shear layer at $x = 17.8$ cm for both upper and lower wires at each of the measurement locations shown in Fig. 1. The upper- and lower-wire trends in rms, skewness, and flatness match one another, indicating good repeatability between runs and hot-wire filaments. The rms exhibits a peak in the central portion of the shear layer and drops off to the rms values corresponding to the Mach-5 and Mach-3 streams at the shear-layer edges. The skewness coefficient is zero (the signal is essentially Gaussian) at the location of peak rms, and then becomes negative near the high-speed edge, and positive near the low-speed edge. The flatness coefficient is about 3.0 (again, a Gaussian signal) at the location of zero skewness and then increases sharply at both shear-layer edges. These trends in rms, skewness, and flatness shown in Fig. 6 are similar to those exhibited in other supersonic shear layers.[5,6]

Power Spectra

A comparison of the power spectra measured at the same relative position within the shear layer at two streamwise locations is shown in Fig. 7. The spectrum at $x = 17.8$ cm is qualitatively similar to spectra measured in incompressible[30] and compressible[28] shear layers because it is relatively flat until about 30 kHz, after which it exhibits a sharp rolloff. The rolloff, however, is steeper than $f^{-5/3}$, as expected for the inertial subrange. The faster rolloff is believed to result from the limited frequency response of the system that is capable of resolving only the largest turbulent scales. In contrast to the upstream spectrum, the spectrum at $x = 48.3$ cm exhibits a pronounced peak, suggesting that there is an increase in energy in the 10- to 40-kHz range with a peak at about 25 kHz. The normalized spectrum in the lower figure also indicates a sharper peak at the downstream station, with the peak at $x = 17.8$ cm being centered at about 30 kHz. Similar results were obtained by Shau et al.[20] from fluctuating pitot pressure data and were attributed to a more organized structure with increasing streamwise distance. The PLS images, however, show that the sharpening of the downstream spectrum is attributable to the development of what appears to be a wake instability, rather than increasing organization of the independent shear layer.

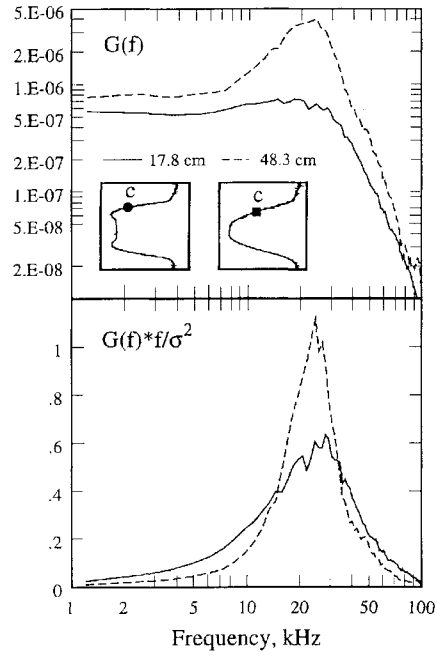

Fig. 7 Comparison of power spectra at x = 17.8 and 48.3 cm.

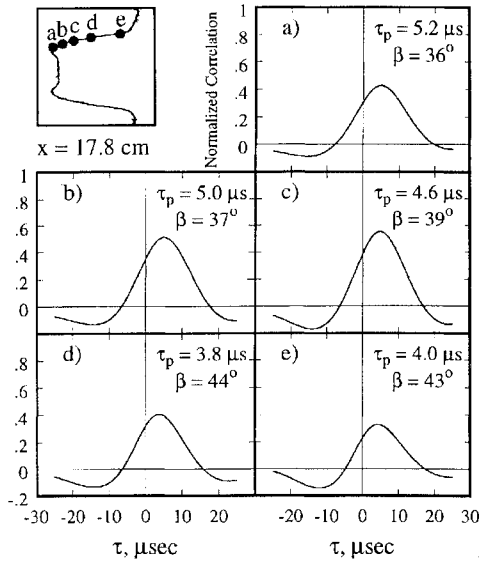

Fig. 8 Average structure angles determined from the standard cross-correlation (x = 17.8 cm, $\Delta y/\delta_{pt}$ = 0.35).

Two-Point Correlations in the x-y Plane

Figure 8 presents cross-correlation curves at each of the five vertical probe midpoint locations a–e at $x = 17.8$ cm. The ratio of vertical wire spacing to shear layer thickness, $\Delta y/\delta_{pt}$, was 0.35. At each vertical location, the time at the peak correlation coefficient τ_p, and the resulting large-scale-structure inclination angle β are indicated. The peak correlation coefficient was found by visual examination of the data. Note that the highest correlation occurs at the shear-layer centerline. Similar cross-correlation curves were obtained at $x = 48.3$ cm.

A summary of the average large-scale-structure inclination angles is shown in Fig. 9. Results are presented at both $x = 17.8$ cm and 48.3 cm and probe spacings of $\Delta y/\delta_{pt} = 0.35$ and 0.60. A trend of increasing inclination angle with increasing vertical location is shown, in agreement with earlier results deduced from fluctuating pitot pressure measurements.[20] At $x = 17.8$ cm, the structure angle ranges from 36 deg at the lower edge to 44 deg at the upper edge. This range of angles is larger than the range of angles measured using the upstream-station PLS images of 15–40 deg. At $x = 48.3$ cm,

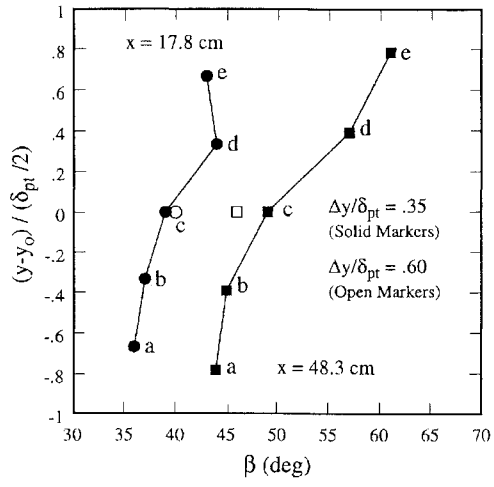

Fig. 9 Average structure inclination angles.

the range of angles inferred from the hot-wire data is 44–60 deg. This range of angles is similar to, but somewhat larger than, the range of angles measured at the same station using the PLS images of 32–55 deg. Also evident from Fig. 9 is a slight difference between the inclination angles obtained with the two different probe spacings (solid markers vs open markers). This difference can be attributed to the fact that the hot-wire probe spacing acts like a filter for structure scales, and that differences in the convection speed can exist between large- and small-scale structures.[31] The $\Delta y/\delta_{pt} = 0.35$ probe spacing is more influenced by structures of smaller scale, and differences in the resulting structure angles are to be expected.

Rajagopalan and Antonia[32] used time-resolved temperature measurements to determine structure inclination angles in a low-speed incompressible shear layer. They found that the average inclination angle of the structures in the shear layer was about 40 deg, which is in good agreement with the present study. They also found, however, that the structure angles peaked near the center of the shear layer, with lower angles occurring near the high- and low-speed edges. This is different from the present results where inclination angles peaked on the high-speed edge of the layer. The reason for this difference is not known, but it may be attributable to the fact that different flowfield variables (i.e., mass flux vs temperature) were measured in the two studies.

Time-delay histograms were produced from the conditional cross-correlation algorithm at each of the five probe locations a–e at 17.8 cm downstream of the origin and are shown in Fig. 10. Each normalized time-delay distribution in Fig. 10 corresponds to a cross-correlation curve in Fig. 8. The average uncorrelated level, discussed previously, is indicated with a thin horizontal line. The number of events comprising each histogram is noted and is lowest at the shear-layer edges because of the intermittent nature of the signal at these locations. Also indicated with a vertical arrow in each figure is the time corresponding to the peak cross-correlation coefficient from Fig. 8. Similar time-delay histograms were obtained for the measurement locations at $x = 48.3$ cm. Good agreement between the peak in the histograms and the time of the peak cross-correlation coefficient is observed in all cases.

Recall that the conditional cross-correlation algorithm produces distributions of time delays between events selectively determined to be indicative of the larger scales. In contrast, the standard cross-correlation contains information from the entire signal—coherent structures of interest as well as incoherent turbulence. What follows now is a closer examination of the standard cross-correlation curves (Fig. 11) and corresponding time-delay histograms (Fig. 12). In each of these three figures, results are presented from data obtained in the central portion of the shear layer. The figures also contain cross-correlation curves and time-delay histograms from data obtained in the undisturbed (empty wind tunnel) Mach-5 tunnel-floor boundary layer for comparison. One probe spacing was employed in the boundary layer, resulting in a ratio of probe spacing to boundary

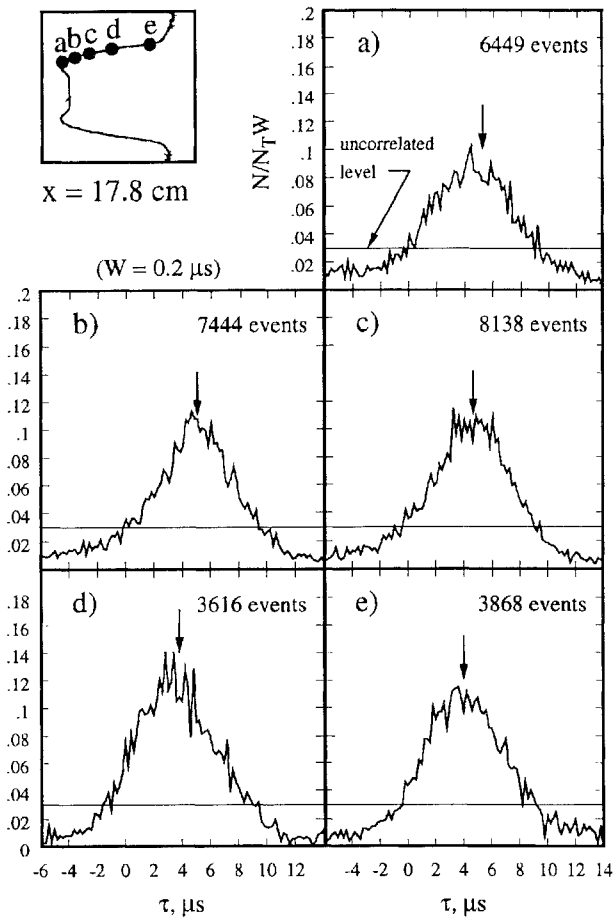

Fig. 10 Time-delay histograms from the conditional cross-correlation algorithm (x = 17.8 cm, $\Delta y/\delta_{pt}$ = 0.35).

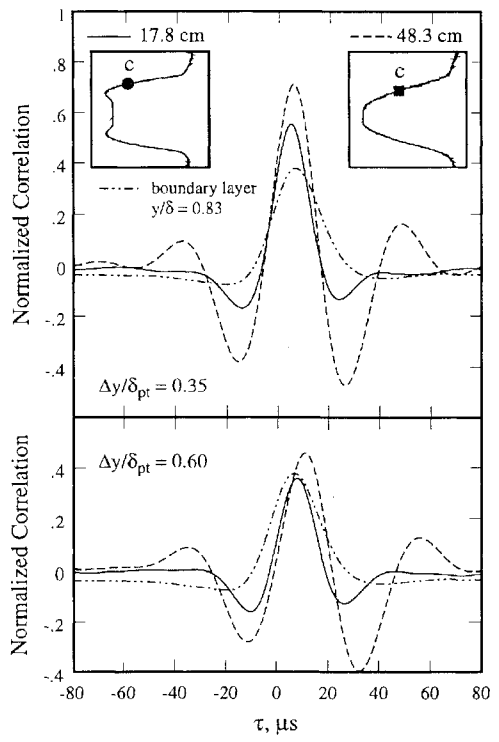

Fig. 11 Cross-correlation curves in the shear layer and the Mach-5 boundary layer.

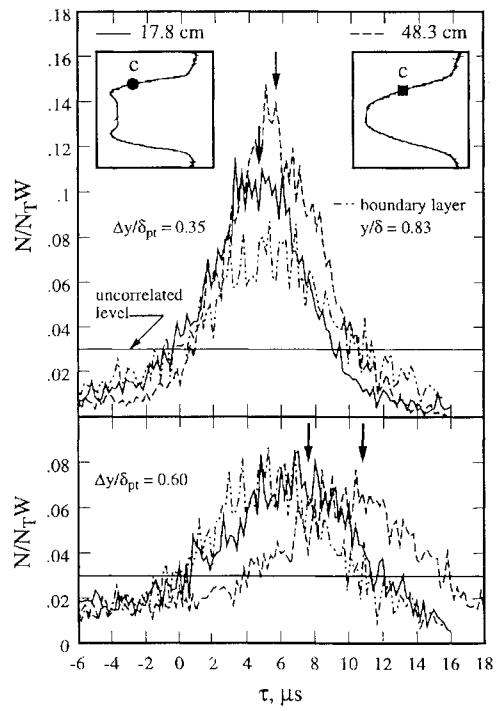

Fig. 12 Time-delay histograms for the boundary layer and the central location of the shear layer.

layer thickness, $\Delta y/\delta$, of 0.30. Cross-correlation curves were computed and the time of the peak correlation coefficient and resulting structure angle were determined. A time-delay range from 9.0 μs near the floor ($y/\delta = 0.33$) to 6.0 μs at $y/\delta = 1.0$ was observed; assuming a structure convection velocity of $0.9U_\infty$, the resulting structure angles are 40 and 52 deg, respectively. This trend of smaller structure angles near the wall is expected in a supersonic boundary layer and has been reported by Spina and Smits[33] and Smits et al.,[34] both at Mach 3. In Figs. 11 and 12, the boundary-layer results at only $y/\delta = 0.83$ are shown for clarity.

Referring to Fig. 11 at $\Delta y/\delta_{pt} = 0.35$, note that the cross-correlation curve for $x = 48.3$ cm has a higher peak correlation coefficient, and larger, more pronounced negative peaks and secondary peaks than that corresponding to $x = 17.8$ cm. The strong negative and secondary peaks are indicative of quasiperiodicity of the turbulent structure. The boundary-layer curve exhibits the lowest correlation peak value and no tails or secondary peaks, suggesting that the boundary-layer structure exhibits no periodic behavior. Similar trends are observed at $\Delta y/\delta_{pt} = 0.60$, where negative tails and a secondary peak are still evident in the shear layer at $x = 48.3$ cm. The peak correlation coefficients for the shear layer have decreased as expected for the larger probe spacing. Note that the boundary-layer curve peak would be lower if a larger probe spacing had been employed there. From these correlation curves, it is evident that a more organized structure exists at $x = 48.3$ cm than at 17.8 cm (consistent with energy spectra and PLS results) and that the shear-layer structure is more organized than the tunnel-floor boundary layer. Cross-correlation results were obtained in incompressible mixing layers by Pui and Gartshore,[31] whose cross correlations exhibited strong negative peaks (similar to those at $x = 48.3$ cm), indicating that their shear layer was more organized than our independent shear layer, while exhibiting an organization similar to that of the interacting shear-layer region of the present study.

Referring again to the cross-correlation curves in Fig. 11, the large-scale structure spacing S can be estimated as $S = U_c \cdot \tau_2 - (\Delta y/\tan\beta)$, where τ_2 is the time delay between the peak cross correlation coefficient and the next secondary peak (40.0 μs at $x = 17.8$ cm and 48.0 μs at $x = 48.3$ cm in this example). For the data obtained at $x = 17.8$ and 48.3 cm, the average structure spacing is 25 mm (3.3 δ_{pt}) and 30 mm (2.3 δ_{pt}), respectively. This change in relative structure spacing is probably related to the different instabilities for the upstream and downstream stations. At a convection velocity of

710 m/s, a structure spacing of 30 mm corresponds to a passage frequency of 24 kHz—matching the peak in the power spectrum shown in Fig. 7.

Figure 12 presents results of the conditional cross-correlation algorithm corresponding to the correlation curves presented in Fig. 11. Note that the most probable structure angle in each histogram matches well with the average angle determined from the standard cross-correlation for both shear-layer locations, as shown by the vertical arrows. At $\Delta y/\delta_{pt} = 0.35$, it seems evident that the same conclusion drawn from the cross-correlation curves in Fig. 11 is valid here. The highest level of correlation occurs at the farthest downstream location in the shear layer. At $\Delta y/\delta_{pt} = 0.60$, the same conclusion cannot be drawn. The correlation level drops as expected in the same manner as the cross-correlation curves; however, no obvious distinction between the curves can be made. A shift to a larger time delay at $x = 48.3$ cm is evident and is attributable to the larger probe spacing used at that location. The level of correlation for the boundary-layer histogram would be lower had a larger probe spacing been employed there for comparison. Nevertheless, it is not obvious from these histograms that the independent shear-layer structure is more organized at 48.3 cm than at 17.8 cm or that the shear layer is more organized than the tunnel-floor boundary layer. This shows the weakness of this statistical technique, since it reveals only subtle differences for a large-scale structure that was shown by the flow visualization to be significantly different.

Two-Point Spanwise Correlations

Spanwise hot-wire data were acquired to assess the two-dimensionality of the large structures. Note that there was not adequate optical access to determine the extent of two-dimensionality using PLS. Cross-correlation curves from data obtained at $x = 48.3$ with use of the hot-wire rake are shown in Fig. 13. The upper set of curves shows a comparison between runs with the same probe spacing, streamwise location (x), and spanwise location (z) but at four vertical (y) positions. All of the curves are essentially the same, characterized by a slight decrease in the peaks and tails at the shear-layer upper and lower edges, consistent with the decrease in intermittency at these locations. A small oblique angle (~10 deg) is evident. Shown in the lower curves are three spanwise correlations from different z locations but the same streamwise and vertical positions.

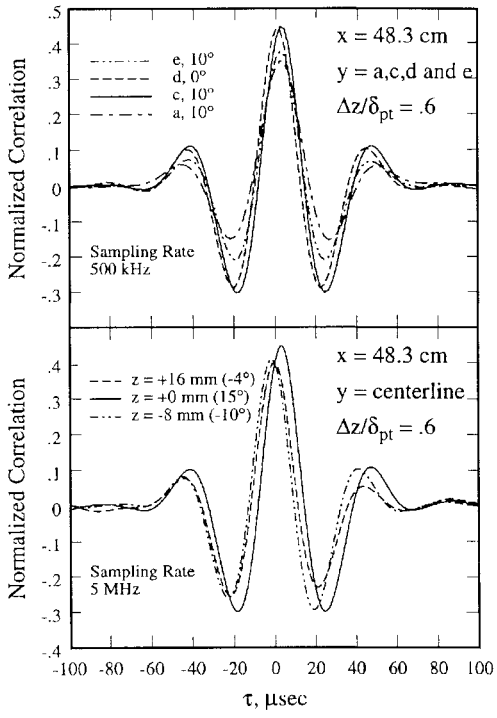

Fig. 13 Vertical and lateral variation of the spanwise correlation and oblique structure angle.

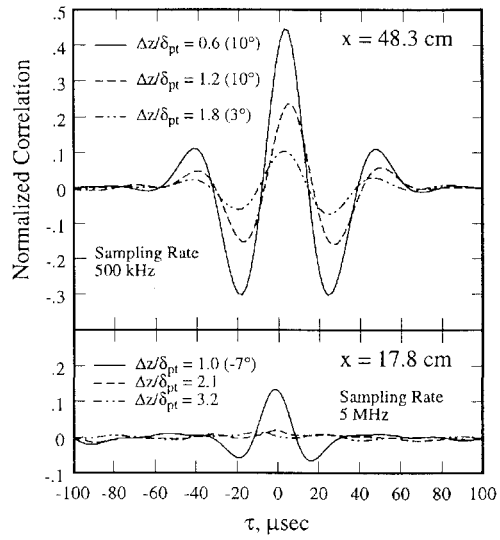

Fig. 14 Comparison of spanwise correlations at two streamwise positions on the shear-layer vertical centerline.

This time, a small shift in the peak time delay, τ_p, is observed. The structure oblique angle is small but varies (±15 deg) with spanwise location.

Variation in the spanwise correlation curves with increasing probe spacing at both downstream locations is shown in Fig. 14. Again, the structure obliquity is small. Obvious from the figure is a rather undeveloped spanwise structure at 17.8 cm downstream of the origin. Plots of the decay of the spanwise correlation peak value with increasing probe spacing show that the spanwise correlation length is about one shear-layer thickness at 17.8 cm, growing to two thicknesses at 48.3 cm.[26] These correlation lengths are comparable to, or larger than, those measured in low-speed incompressible shear layers.[27,30,33,35] Given the flow visualization evidence of reduced organization in this shear layer, it seems unlikely that it is more two-dimensional than the incompressible shear layers that exhibited smaller correlation lengths but were otherwise found to be highly organized.[35] The relatively large correlation lengths of the present study may be attributable to the limited frequency response of the system and the relatively large length of the probe (1 mm), which will tend to filter out the small scales that act to reduce correlation coefficients.[27]

Discussion of Results

For the upstream measurements in the independent shear layer, both the hot-wire results and the PLS imaging showed that the shear layer is quite unorganized. If M_c is the most important parameter for determining the shear-layer structure, then this is an unexpected result owing to the low convective Mach number (0.28), particularly considering the large $x/\theta_o (= 1600)$, and the low local Reynolds number $Re_\delta = 4 \times 10^4$. This Reynolds number is several times lower than in incompressible shear-layer studies where strong organization was observed,[35–38] even when originating from a splitter plate with turbulent boundary layers.[35,36,38] The probable reason for this is that the shear layer, despite the large x/θ_o, has not fully recovered from its (highly unorganized) initial conditions. Browand and Troutt[36] found that the turbulent structure in incompressible shear layers becomes independent of downstream distance for $x/\theta_o \approx 400(1 + U_2/U_1)/(1 - U_2/U_1)$. This relation shows that as a shear layer approaches a wake (as $U_2/U_1 \to 1$), it requires an increasing distance downstream to become fully developed. For the present shear layer, where $U_2/U_1 = 0.84$, the above relation gives a development distance of $4600\,\theta_o$, which is significantly larger than even the farthest downstream location available. Assuming that the same relation holds for supersonic shear layers, then this suggests that the independent shear layer may not have recovered from the unorganized turbulence of the initial high-speed boundary layer. One way of interpreting this is to consider the ratio of the turbulent structure time of flight (x/U_c) to the eddy turnover

time ($\delta/\Delta U$). This ratio decreases as U_2/U_1 approaches unity, indicating that the large scales at a given downstream station have less time to develop. This has particular importance for supersonic shear-layer studies because low-convective-Mach-number conditions are typically achieved by accelerating both streams to high Mach numbers.

The increase in organization with increasing downstream distance that was found by Shau et al.[20] was shown by the PLS to be attributable to the interaction of the two shear layers to form a new apparently wake-like instability. This new instability exhibits a sharp peak in the power spectra and has approximately twice the spanwise correlation length as the upstream shear layer.

Both the PLS and the hot-wire results indicate a significant increase in the characteristic structure angle from the upstream to the downstream location. The increase was 39 and 28%, for the PLS and hot-wire measurements, respectively. This increase in the structure angle is undoubtedly related to the development of the new instability at the downstream location. Even though the trend was similar, the angles measured using the PLS and the hot wires differed substantially: The angle measured at the upstream location using PLS was 28% lower than that measured using the hot wires on centerline, whereas at the downstream location the PLS result was 16% lower. The reason for the difference between the PLS and probe measurements is not known, but it may reflect the fact that the angles determined using the image data are biased toward structures where angles could be visually observed, whereas the standard cross-correlation technique gives angles that have contributions from all resolvable structures. It is also possible, however, that the two techniques do not detect the same structures that are responsible for the characteristic angle. This is possible because the concentration of the passive scalar is not directly related to the velocity field and is strongly influenced by the mixing history.

Conclusions

Flow visualization and time series analysis of hot-wire signals were used to investigate the structure of two adjacent planar shear layers bounded by Mach-5 and Mach-3 streams, giving a convective Mach number of 0.28. The major conclusions include the following:

1) The flow visualization and hot-wire results indicate that the large-scale structure in the near-field independent shear layers is more unorganized than that found in previous studies of incompressible and low-convective-Mach-number supersonic shear layers at the same or higher Reynolds numbers. The reason for this is believed to be attributable to the observation in incompressible shear layers that as U_2/U_1 approaches unity an increasing streamwise distance is required to attain a fully developed state.

2) Power spectra sharpen with increasing streamwise distance, indicating an increase in organization. This increased organization was shown by the flow visualization to be attributable to the shear layers interacting to form an apparent wake-like instability characterized by a vortex street.

3) The hot-wire measurements show that the large-scale structures are inclined in the x-y plane with a range of angles from 36 to 43 deg for the independent shear layers, and from 44 to 60 deg for the interacting shear layers. Characteristic angles measured from the images are about 27% lower than the hot-wire results for the independent shear layers, but are only 14% lower for the interacting layers.

Acknowledgments

Support from the U.S. Office of Naval Research under Grant N0014-89-J-1221, monitored by P. Purtell and S. Lekoudis, is gratefully acknowledged. We would also like to thank E. Lachney and S. C. Chan for acquiring the image data.

References

[1]Kumar, A., Bushnell, D. M., and Hussaini, M. Y., "Mixing Augmentation Technique for Hypervelocity Scramjets," AIAA Paper 87-1882, 1987.

[2]Menon, S., "Shock Waves for Enhanced Mixing in Scramjet Combustors," National Aerospace Plane CR 1028, Dec. 1988.

[3]Bogdanoff, D. W., "Compressibility Effects in Turbulent Shear Layers," *AIAA Journal*, Vol. 21, No. 6, 1983, pp. 926, 927.

[4]Papamoschou, D., and Roshko, A., "The Compressible Turbulent Shear Layer: An Experimental Study," *Journal of Fluid Mechanics*, Vol. 197, 1988, pp. 453–477.

[5]Elliott, G. S., and Samimy, M., "Compressibility Effects in Free Shear Layers," *Physics of Fluids*, Vol. 2, No. 7, 1990, pp. 1231–1240.

[6]Goebel, S. G., and Dutton, J. C., "Experimental Study of Compressible Turbulent Mixing Layers," *AIAA Journal*, Vol. 29, No. 4, 1991, pp. 538–546.

[7]Clemens, N. T., and Mungal, M. G., "Two- and Three-Dimensional Effects in the Supersonic Mixing Layer," *AIAA Journal*, Vol. 30, No. 4, 1992, pp. 973–981.

[8]Hall, J. L., Dimotakis, P. E., and Roseman, H., "Experiments in Non-Reacting Compressible Shear Layers," AIAA Paper 91-0629, 1991.

[9]Bonnet, J. P., Debisschop, J. R., and Chambres, O., "Experimental Studies of the Turbulent Structure of Supersonic Mixing Layers," AIAA Paper 93-0217, 1993.

[10]Messersmith, N. L., Dutton, J. C., and Krier, H., "Experimental Investigation of Large Scale Structures in Compressible Mixing Layers," AIAA Paper 91-0244, 1991.

[11]Elliott, G. S., Samimy, M., and Arnette, S. A., "Study of Compressible Mixing Layers with Filtered Rayleigh Scattering Based Visualizations," *AIAA Journal*, Vol. 30, No. 10, 1993, pp. 2567–2569.

[12]Samimy, M., Reeder, M. F., and Elliott, G. S., "Compressibility Effects on Large Structures in Free Shear Flows," *Physics of Fluids*, Vol. 4, No. 6, 1992, pp. 1251–1258.

[13]Samimy, M., and Addy, A. L., "Interaction Between Two Compressible, Turbulent Free Shear Layers," *AIAA Journal*, Vol. 24, No. 12, 1986, pp. 1918–1923.

[14]Dutton, J. C., Herrin, J. L., Molezzi, M. J., Mathur, T., and Smith, K. M., "Recent Progress on High-Speed Separated Base Flows," AIAA Paper 95-0472, 1995.

[15]Althaus, W., "Experimental Investigation of Vortex Formation in the Wake of a Flat Plate for Subsonic and Supersonic Freestream Mach Numbers," *Experiments in Fluids*, Vol. 9, 1990, pp. 267–272.

[16]Bonnet, J. P., and Chaput, E., "Large-Scale Structures Visualization in a High Reynolds Number, Turbulent Flat-Plate Wake at Supersonic Speeds," *Experiments in Fluids*, Vol. 4, 1986, pp. 350–356.

[17]Bonnet, J. P., Jayaraman, V., and Alziary de Roquefort, T., "Structure of a High-Reynolds-Number Turbulent Wake in Supersonic Flow," *Journal of Fluid Mechanics*, Vol. 143, 1984, pp. 277–304.

[18]Weir, A. D., Wood, D. H., and Bradshaw, P., "Interacting Turbulent Shear Layers in a Plane Jet," *Journal of Fluid Mechanics*, Vol. 107, 1981, pp. 237–260.

[19]Shau, Y. R., "Experimental Study of Growth Rate Enhancement and Structure of Compressible Turbulent Free Shear Layers," Ph.D. Dissertation, Dept. of Aerospace Engineering and Engineering Mechanics, Univ. of Texas, Austin, TX, 1990.

[20]Shau, Y. R., Dolling, D. S., and Choi, K. Y., "Organized Structure in a Compressible Turbulent Shear Layer," *AIAA Journal*, Vol. 31, No. 8, 1993, pp. 1398–1405.

[21]Ramamoorthy, S., Munukutla, S., and Rajan, P. K., "Relation Between Spectra of Hotwire Anemometer Fluctuating Voltages and Those of the Turbulence Quantities," AIAA Paper 92-3958, 1992.

[22]McGregor, I., "The Vapor Screen Method of Flow Visualization," *Journal of Fluid Mechanics*, Vol. 11, 1961, pp. 481–511.

[23]Clemens, N. T., and Mungal, M. G., "A Planar Mie Scattering Technique for Visualizing Supersonic Mixing Flows," *Experiments in Fluids*, Vol. 11, 1991, pp. 175–185.

[24]Samimy, M., and Lele, S. K., "Motion of Particles with Inertia in a Compressible Free Shear Layer," *Physics of Fluids*, Vol. 3, No. 8, 1991, pp. 1915–1923.

[25]Bendat, J. S., and Piersol, A. G., *Random Data: Analysis and Measurement Procedures*, 2nd ed., Wiley, New York, 1986, Chap. 11.

[26]Petullo, S. P., and Dolling, D. S., "Large-Scale Structure Orientation in a Compressible Turbulent Shear Layer," AIAA Paper 93-0545, 1993.

[27]Jones, B. G., Planchon, H. P., and Hammersley, R. J., "Turbulent Correlation Measurements in a Two-Stream Mixing Layer," *AIAA Journal*, Vol. 11, No. 8, 1973, pp. 1146–1150.

[28]Ikawa, H., and Kubota, T., "Investigation of Supersonic Turbulent Mixing Layer with Zero Pressure Gradient," *AIAA Journal*, Vol. 13, No. 5, 1975, pp. 566–572.

[29]Seitzman, J. M., Miller, M. F., Island, T. C., and Hanson, R. K., "Double-Pulse Imaging Using Simultaneous OH/Acetone PLIF for Studying the Evolution of High-Speed Reacting Mixing Layers," *Twenty-Fifth Symposium* (International) *on Combustion*, Combustion Inst., Pittsburgh, PA, 1995, pp. 1743–1750.

[30]Champagne, F. H., Pao, Y. H., and Wygnanski, I. J., "On the Two-Dimensional Mixing Region," *Journal of Fluid Mechanics*, Vol. 74, 1976, pp. 209–250.

[31]Pui, N. K., and Gartshore, I. S., "Measurements of the Growth Rate and Structure in Plane Turbulent Mixing Layers," *Journal of Fluid Mechanics*, Vol. 91, 1979, pp. 111–130.

[32]Rajagopalan, S., and Antonia, R. A., "Properties of the Large Structure in a Slightly Heated Turbulent Mixing Layer of a Plane Jet," *Journal of Fluid Mechanics*, Vol. 105, 1981, pp. 261–281.

[33]Spina, E. F., and Smits, A. J., "Organized Structures in a Compressible Turbulent Boundary Layer," *Journal of Fluid Mechanics*, Vol. 182, 1986, pp. 85–109.

[34]Smits, A. J., Spina, E. F., Alving, A. E., Smith, R. W., Fernando, E. M., and Donovan, J. F., "A Comparison of the Turbulence Structure of Subsonic and Supersonic Boundary Layers," *Physics of Fluids*, Vol. 1, No. 11, 1989, pp. 1865–1875.

[35]Wygnanski, I., Oster, D., Fiedler, H., and Dziomba, B., "On the Perseverence of a Quasi-Two-Dimensional Eddy-Structure in a Turbulent Mixing Layer," *Journal of Fluid Mechanics*, Vol. 93, 1979, pp. 325–335.

[36]Browand, F. K., and Troutt, T. R., "The Turbulent Mixing Layer: Geometry of the Large Vortices," *Journal of Fluid Mechanics*, Vol. 158, 1985, pp. 489–509.

[37]Dimotakis, P. E., and Brown, G. L., "The Mixing Layer at High Reynolds Number: Large-Structure Dynamics and Entrainment," *Journal of Fluid Mechanics*, Vol. 78, 1976, pp. 535–560.

[38]Mungal, M. G., Hermanson, J. C., and Dimotakis, P. E., "Reynolds Number Effects on Mixing and Combustion in a Reacting Shear Layer," *AIAA Journal*, Vol. 23, No. 9, 1985, pp. 1418–1423.